PAPER

Check for updates

Template-free synthesis of a multilayer manganese oxide/graphene oxide nanoflake-modified carbon felt as an anode material for microbial fuel cells†

Lizhen Zeng [iD] *[a] and Lixia Zhang[b]

A novel multilayer nanoflake structure of manganese oxide/graphene oxide (γ-MnO$_2$/GO) was fabricated *via* a simple template-free chemical precipitation method, and the modified carbon felt (CF) electrode with γ-MnO$_2$/GO composite was used as an anode material for microbial fuel cells (MFCs). The characterization results revealed that the γ-MnO$_2$/GO composite has a novel multilayer nanoflake structure and offers a large specific surface area for bacterial adhesion. The electrochemical analyses demonstrated that the γ-MnO$_2$/GO composite exhibited excellent electrocatalytic activity and enhanced the electrochemical reaction rate and reduced the electron transfer resistance, consequently facilitating extracellular electron transfer (EET) between the anode and bacteria. The maximum power density of MFC equipped with the γ-MnO$_2$/GO composite-modified carbon felt anode was 1.13 ± 0.09 W m^{-2}, which was 119% higher than that of the pure commercial carbon felt anode under the same conditions. Thus, the results demonstrate that the multilayer γ-MnO$_2$/GO nanoflake composite-modified carbon felt anode is a promising anode material for high-performance MFC applications.

Microbial fuel cells (MFCs) are renewable energy devices that utilize microorganisms as biocatalysts to oxidize and decompose organic substrates, thereby generating electrical energy.[1–4] This environmentally friendly technology simultaneously addresses the problems of wastewater treatment and energy generation. However, the power density of MFCs at present is relatively low, which is several orders of magnitude lower than that of the traditional batteries. Their practical application is still beyond reach, and the devices need to be further improved.[5–8]

Due to the attachment of bacteria to the anode, the properties of anode not only affect the amount of bacterial adhesion but also influence the efficiency of electron transfer between bacteria and the anode.[3] Therefore, the choice of anode material plays a very important role in improving the performance of MFCs.[4,9–12] Consequently, the ideal anode material should possess high chemical and physical stability, high conductivity, high specific surface area, low cost, non-corrosive nature and good biocompatibility.[3] Owing to their excellent biocompatibility and low cost, carbon-based materials are widely used as the most common anode materials in MFCs.[13,14] However, the

relatively smooth surface of conventional carbon-based materials is not conducive to the attachment of bacteria, and their low conductivity also limits the performance of MFCs. An effective way to solve this problem is to modify carbon-based materials with metals, metal oxides, or carbides.[3,15–17]

Transition metal oxide MnO$_2$ has gained much attention in the construction of MFCs, owing to its theoretical specific capacitance ($\sim$1370 F g^{-1}), superior biocompatibility, environmental friendliness and low cost.[18–22] Zhang *et al.* have proved that MnO$_2$ particles and rGO/MnO$_2$ composite deposited on the surface of carbon felt can promote electrode reaction and electron transfer, thereby enhancing the performance of MFCs.[18,19] Pure MnO$_2$ typically has a relatively low surface area (10–80 m^2 g^{-1}) and exhibits poor electronic conductivity, which restricts its electrochemical performance.[20–22] It is commonly known that graphene oxide (GO) has a large surface area (400–1500 m^2 g^{-1}), good electrical conductivity, and excellent dispersion in aqueous media.[23,24] Combining the advantages of GO and MnO$_2$ can effectively enhance the electrical conductivity and specific surface area of MnO$_2$.[19,21] Many methods are used to fabricate MnO$_2$/GO composite, including electrodeposition method, hydrothermal method and chemical precipitation method.[19,21,22] Compared with these methods, the template-free synthesis method has multiple advantages of cost-effectiveness, simplified synthesis process, high efficiency, and environmental friendliness.

Herein, we fabricated multilayer γ-MnO$_2$/GO nanoflakes using a facile template-free chemical precipitation method. The

[a]Analysis and Testing Center, South China Normal University, Guangzhou 510006, China. E-mail: zenglizhen@m.scnu.edu.cn

[b]CAS Key Laboratory of Environmental and Applied Microbiology, Environmental Microbiology Key Laboratory of Sichuan Province, Chengdu Institute of Biology, Chinese Academy of Sciences, Chengdu 610041, China

γ-MnO$_2$/GO composite, with its unique multilayer nanoflake structure and superior biocompatibility, offers a large specific surface area for bacterial adhesion and exhibits excellent electrochemical performance. By combining the advantages of γ-MnO$_2$ and GO, the MFC equipped with the γ-MnO$_2$/GO composite-modified carbon felt anode performs better than a pure carbon felt anode under the same conditions.

1 Materials and methods

1.1 Preparation of multilayer γ-MnO$_2$/GO nanoflake composite

The γ-MnO$_2$/GO composite with a novel multilayer nanoflake structure was fabricated using a facile chemical precipitation method without the use of any template: 0.02 g of graphite oxide (GO) was dissolved in 20 mL of deionized (DI) water, and uniformly dispersed for 2 h to form a stable GO colloid. GO was prepared using a modified Hummers' method.[25,26] Then, 0.2 g of MnCl$_2$·4H$_2$O was added and stirred for 1 h. Subsequently, 0.24 g of KMnO$_4$ dissolved in DI water (20 mL) was slowly added dropwise into the above solution under ultrasonication for 6 h. Finally, the γ-MnO$_2$/GO composite was obtained by filtering, washing several times with DI water and ethanol, and drying in a vacuum overnight at 80 °C. For comparison, pure γ-MnO$_2$ was prepared using the same method, but without adding graphite oxide.

1.2 Materials characterization

The morphology and structure of the samples and biofilm were characterized using a field-emission scanning electron microscope (FESEM, ZESISS ULTRA 55, Germany) and high-resolution transmission electron microscopy (HRTEM, JEOL JEM-2100, Japan). The XPS spectra were carried out on ESCALAB 250 (Thermo Fisher Scientific, USA) using monochromatic Al Kα radiation (1486.6 eV). The XRD patterns of the samples were determined using a D8 Advance X-ray diffractometer (XRD, Bruker D8 Advance, Germany) with Cu Kα radiation ($\lambda = 1.5405$ nm), and the test angle range was 10–80°. The Raman spectra of samples were recorded using a confocal microscope Raman spectrometer system (Lab RAM Aramis, HORIBA, France). N$_2$ adsorption/desorption experiments were conducted using an N$_2$ adsorption/desorption analyzer (Micrometrics, ASAP 2020, USA), and the specific surface area, pore volume, and pore size of the samples were calculated according to the Brunauer–Emmett–Teller (BET) equation and the Barrett–Joyner–Halenda (BJH) adsorption model.

1.3 MFC construction, operation and tests

An air-cathode cylindrical MFC was constructed, as previously reported.[27] The γ-MnO$_2$/GO composite was coated on one side of a CF electrode (2.0 cm × 2.0 cm) with poly(tetrafluoroethylene) solution (1 wt%) to obtain the γ-MnO$_2$/GO/CF anode. The MnO$_2$/CF was prepared by the same method, and a pure carbon felt anode was used for comparison. The anode (2.0 cm × 2.0 cm × 0.1 cm) and the cathode were both connected with titanium wires to form a closed circuit through an external resistance of 1000 Ω. The cathode was prepared as previously reported,[12] and the cathode catalyst was Pt/C with Pt loading of 0.5 mg cm^{-2}.

For MFC start-up, the reactor was inoculated with 5.0 mL of effluent of a matured single-chamber MFC anolyte and 23 mL of sodium acetate (1 g L^{-1}) culture medium solution.[11,13] The MFC experiment was conducted in a batch mode at 30 °C in an incubator. The culture medium solution contained a vitamin solution (12.5 mL L^{-1}) and a mineral solution (12.5 mL L^{-1}) in 50 mM phosphate buffer solution (pH 7.0). Polarization curves were obtained by varying the external resistance at the stable state of the MFCs from 100 to 8000 Ω.

Electrochemical tests in a three-electrode half-cell were conducted on a Solartron 1480 (Solartron Analytic, England) using the anode as the working electrode, a saturated calomel electrode (SCE) as the reference electrode, and a titanium wire as the counter electrode. Chronoamperometry (CA) was performed by setting the anodic potential to +0.2 V (vs. SCE), and recording the changes in the response current; the variation in current values can indicate the strength of electron transfer in the system and the level of electrode reactivity. Cyclic voltammograms (CV) were carried out within the range of −0.6 V to 0.3 V (vs. SCE) at a scan rate of 10 mV s^{-1}. Chronopotentiometry (CP) was conducted after the formation of a stable biofilm at a current of 0.1 μA. Electrochemical impedance spectroscopy (EIS) was performed at the open-circuit voltage of the MFC, with a frequency range of 10^5 to 10^{-2} Hz and an amplitude of 5 mV, on an electrochemical workstation (Autolab PGSTAT-302N, Metrohm Autolab, Switzerland).

2 Results and discussion

2.1 Characterization of the multilayer γ-MnO$_2$/GO nanoflake composite

Fig. 1 illustrates the schematic diagram of the self-assembled γ-MnO$_2$/GO nanoflake composite. As shown in Fig. 1, the multilayer γ-MnO$_2$/GO nanoflake composite is fabricated via a facile template-free chemical precipitation method, and γ-MnO$_2$ is prepared using the same method but without adding graphite oxide and template. SEM images and TEM images can further confirm that γ-MnO$_2$ has a nano-flower structure, and γ-MnO$_2$/GO has a multilayer nanoflake structure. Fig. 2a and b show the SEM images of γ-MnO$_2$ and the γ-MnO$_2$/GO composite, respectively. It can be observed easily from Fig. 2a that γ-MnO$_2$ is a typical aggregated nano-flower structure with many wrinkles on the surface, and the diameter of the nanoflowers ranges from 0.5 to 1 μm. As shown in Fig. 2b, the γ-MnO$_2$ nanoflakes are loosely assembled and tightly anchored to both sides of the GO sheets, indicating that the γ-MnO$_2$/GO composite has a multilayer nanoflake structure. The TEM images (Fig. 2c) further confirm the nano-flower structure of γ-MnO$_2$, and indicate that the γ-MnO$_2$ nano-flower is actually composed of nanoflakes. The TEM image of the γ-MnO$_2$/GO composite (Fig. 2d) shows that the γ-MnO$_2$ nanoflakes are uniformly embedded on the surface of the GO sheets, which indicates that the GO sheets can provide not only abundant active sites for the nucleation of γ-MnO$_2$, but also serve as a support for the growth
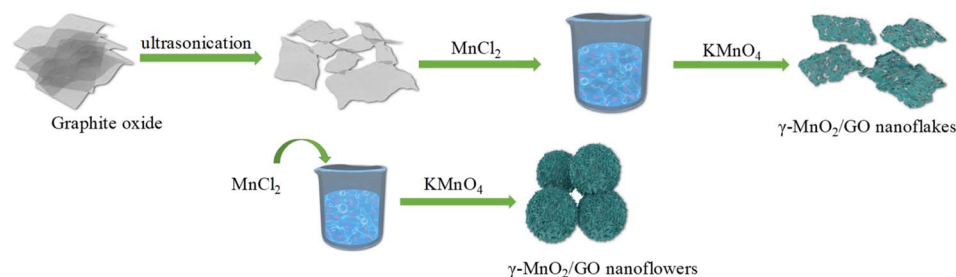
Fig. 1 Schematic diagram of the synthesis of the self-assembled γ-MnO$_2$/GO nanoflakes and γ-MnO$_2$ nanoflowers.

of γ-MnO$_2$. Fig. S1† shows the TEM image and selected area electron diffraction (SAED) of GO. As demonstrated in Fig. S1,† GO is a transparent and flat sheet. The presence of the GO sheet effectively prevents the γ-MnO$_2$ nanoflakes from self-assembling into γ-MnO$_2$ nanoflower structure.[21] From the HRTEM image (Fig. 2e), the lattice spacing of the particles matches that of γ-MnO$_2$, indicating that the particles are γ-MnO$_2$ nanoparticles. The SAED result (Fig. 2f) shows distinct diffraction rings, and there are a large number of bright spots on the rings, indicating that the nanoparticles have a poly-crystalline structure.

X-ray diffraction (XRD) patterns confirm the crystal structures of pure γ-MnO$_2$ and the γ-MnO$_2$/GO composite, as shown in Fig. S2a.† The characteristic diffraction peaks of pure γ-MnO$_2$
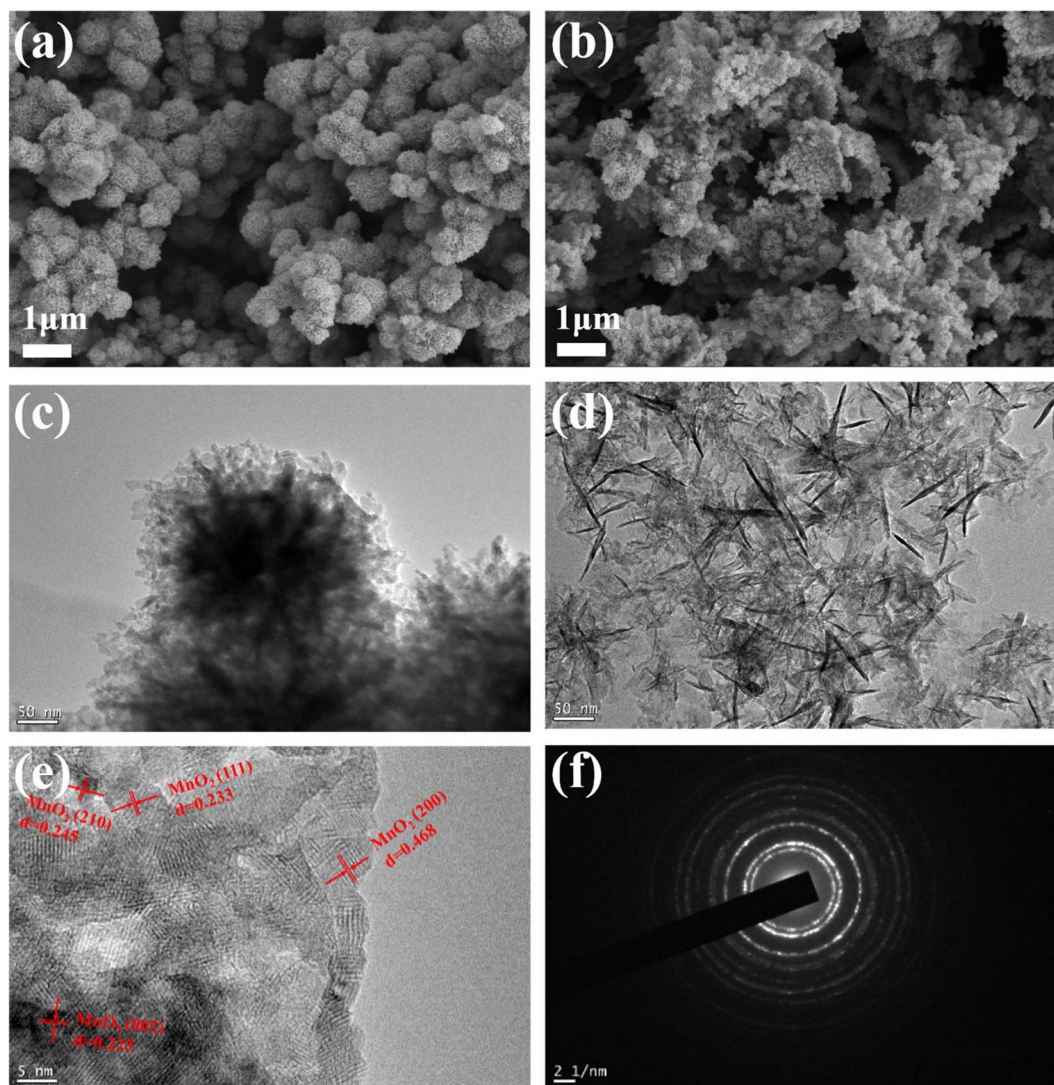
Fig. 2 SEM images of γ-MnO$_2$ (a) and γ-MnO$_2$/GO composite (b); TEM images of γ-MnO$_2$ (c) and γ-MnO$_2$/GO composite (d); HRTEM image (e) and SAED (f) of γ-MnO$_2$/GO composite.

at around 22.0°, 36.8°, 42.2°, 55.4° and 66.3° can be indexed to the (101), (210), (211), (212) and (020) planes of γ-MnO$_2$, respectively (JCPDS 44-0142).[28] The same diffraction peaks can also be observed in the γ-MnO$_2$/GO composite. However, it should be noted that no diffraction peaks related to aggregated GO ($2\theta = 12.2°$, corresponding to the (002) crystal plane of graphite) were observed in the γ-MnO$_2$/GO composite material sample, indicating that the content of GO in the composite is relatively low and the γ-MnO$_2$ nanoflakes have been uniformly embedded in GO, preventing the aggregating of GO into the graphite sheets.[20,29] The Raman spectra of the γ-MnO$_2$/GO composite, pure γ-MnO$_2$, and GO are shown in Fig. S2b.† The D band at 1347 cm^{-1} and G band at 1588 cm^{-1} of the oxidized graphite can be detected in the pure GO spectrum. Furthermore, the Mn–O stretching vibration band at 633 cm^{-1} is observed in the pure MnO$_2$ spectrum.[21] Notably, the γ-MnO$_2$/GO composite has the characteristics of both GO and MnO$_2$, further indicating that the hybrid structure is composed of GO and γ-MnO$_2$.[21,30]

Fig. 3 shows the N$_2$ adsorption–desorption isotherm curves of γ-MnO$_2$ and the γ-MnO$_2$/GO composite, both of which exhibit typical Type IV characteristics. The corresponding specific surface area of the γ-MnO$_2$/GO composite and γ-MnO$_2$ are approximately 127.29 m^2 g^{-1} and 87.20 m^2 g^{-1}, respectively. Furthermore, the pore volume of the γ-MnO$_2$/GO composite (0.36 cm^3 g^{-1}) is higher than that of γ-MnO$_2$ (0.23 cm^3 g^{-1}). Electrode materials with a larger specific surface area can

adsorb and accommodate more bacteria on their surface, which can generate more extracellular electrons, thereby enhancing the performance of MFCs.[12] Therefore, the γ-MnO$_2$/GO composite provides a larger specific surface area for reactions, enhances interfacial transport, and offers a biocompatible interface that is conducive to bacterial adhesion and substrate transport.[6,31]

Important information on the surface compositions and electronic states of the γ-MnO$_2$/GO composite can be further revealed by X-ray photoelectron spectroscopy (XPS). As shown in Fig. 4a, the XPS spectra confirm the presence of Mn, C and O elements. The high-resolution C 1s spectrum in Fig. 4b can be deconvolved into three peaks, each corresponding to carbon atoms in three functional groups: sp^2 hybridized carbon (C–C, 284.6 eV), epoxy/hydroxyls groups (C–O, 285.3 eV), and carbonyl groups (C=O, 288.2 eV).[32] The strong peak at 284.3 eV is associated with the graphitic carbon in graphene oxide. The high-resolution Mn 2p spectrum (Fig. 4c) displays two signals at 641.9 eV and 653.6 eV, corresponding to Mn 2p$_{3/2}$ and 2p$_{1/2}$ peaks, respectively, which are characteristic of typical MnO$_2$.[22] The O 1s spectrum (Fig. 4d) contains three peaks, which are attributed to the O–Mn in MnO$_2$ at the lower binding energy (529.4 eV), GO functional groups at a higher binding energy (530.8 eV) and 532.2 eV.[33] EDS analysis is further used to confirm that the prepared sample contains Mn, C and O elements (Fig. S3†). Moreover, as shown in Fig. 4e–h, the EDS element mapping analysis was used to confirm the presence of
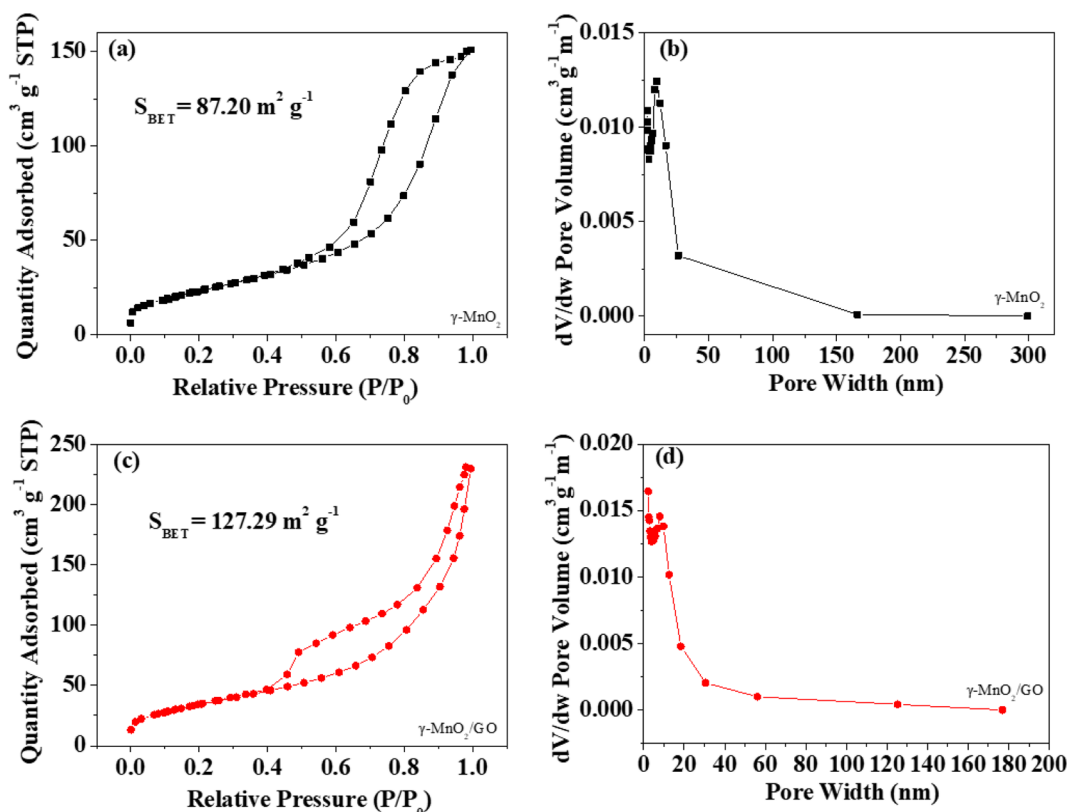

Fig. 3 Nitrogen adsorption–desorption isotherms of γ-MnO$_2$ (a) and γ-MnO$_2$/GO composite (c); corresponding pore-size distribution curves of γ-MnO$_2$ (b) and γ-MnO$_2$/GO composite (d).

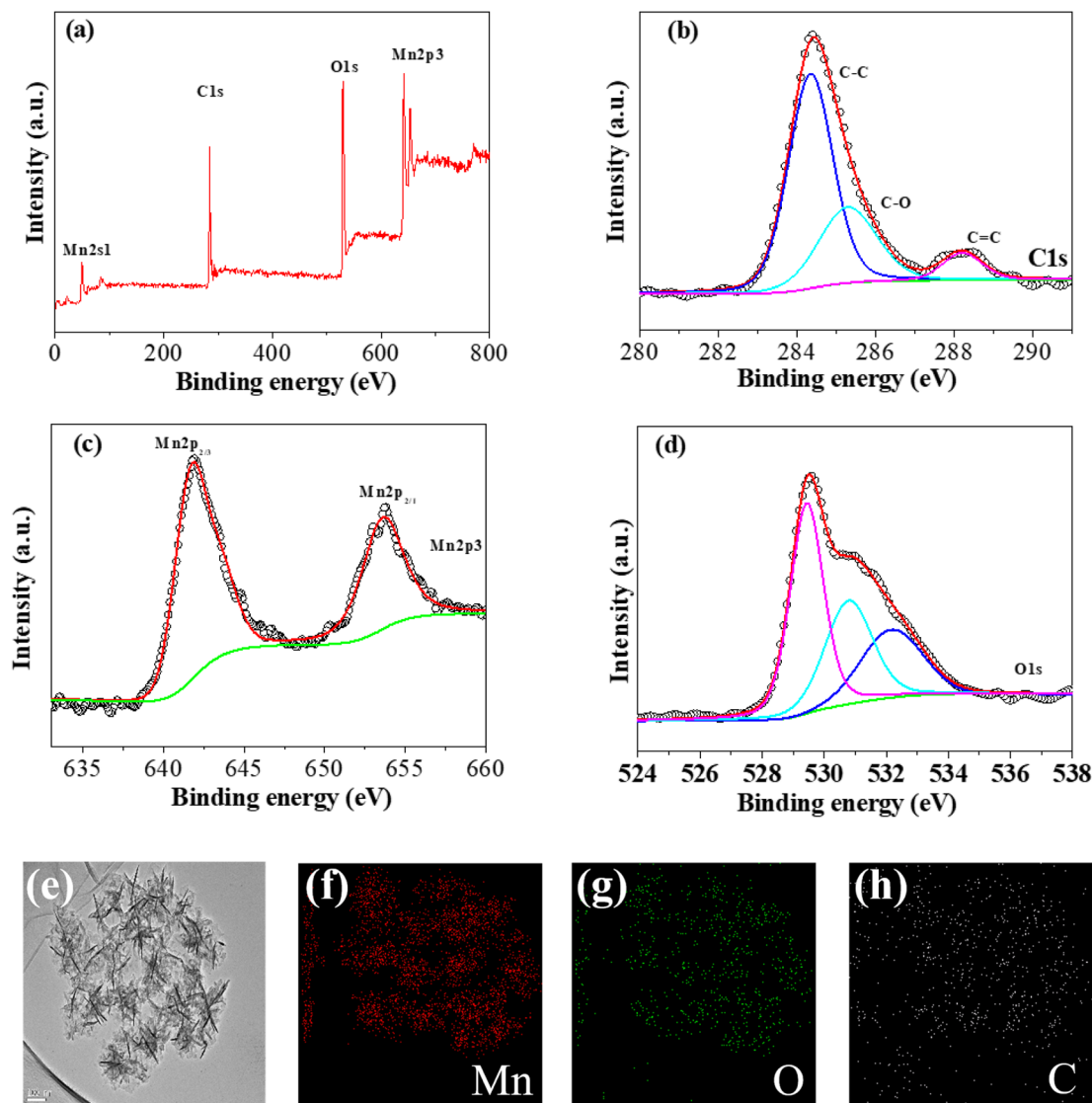**Fig. 4** XPS spectra of γ-MnO$_2$/GO composite (a); high-resolution C 1s (b), Mn 2p (c), and O 1s (d) spectra of γ-MnO$_2$/GO composite; TEM image of γ-MnO$_2$/GO (e) and corresponding quantitative EDS elemental mappings of Mn (f), O (g), and C (h).

Mn, O and C elements, and these elements are uniformly distributed in the composite.

2.2 MFC performances

The γ-MnO$_2$/GO/CF and γ-MnO$_2$/CF electrodes were used as the anodes for power generation over multiple working cycles in single-chamber air cathode MFCs, with an external resistance of 1000 Ω, and were compared to the pure CF electrode. The batch-fed MFC was inoculated with a 5.0 mL of effluent from the anode electrolyte of a matured single-chamber MFC, and then operated using sodium acetate as the sole anodic electron donor at a concentration of 10 mmol L^{-1}. As shown in Fig. 5a, the MFC equipped with the γ-MnO$_2$/GO/CF anode exhibits the earliest start-up at around 150 h, while the MFC equipped with pure CF anode has the slowest start-up. After a successful start-up, upon replenishing MFC with fresh substrate, the cell voltage rapidly increases to its maximum value, and then gradually

decreases as the sodium acetate in the anode solution is consumed. Notably, it is also observed that the γ-MnO$_2$/GO/CF anode delivers the highest cell voltage.

After 3 weeks of stable operation of the MFCs, the power production and polarization behaviour of the MFCs were investigated, as shown in Fig. 5b. The results indicate that the anode material has a significant impact on power density, but has no significant effect on open circuit voltage. As illustrated in Fig. 5b, the maximum power density of MFC equipped with the γ-MnO$_2$/GO/CF anode is 1.13 ± 0.09 Wm^{-2}, which is 71.2% and 119% higher than that of the γ-MnO$_2$/CF anode (0.660 ± 0.10 W m^{-2}) and the pure CF anode (0.516 ± 0.026 W m^{-2}), respectively.[13] Table S1† shows a comparison of the MFC performance with different anode materials under the same type of air-cathode cylindrical MFC and inoculum conditions. The results indicate that the performance of the γ-MnO$_2$/GO/CF electrode is superior to all electrodes, except for the
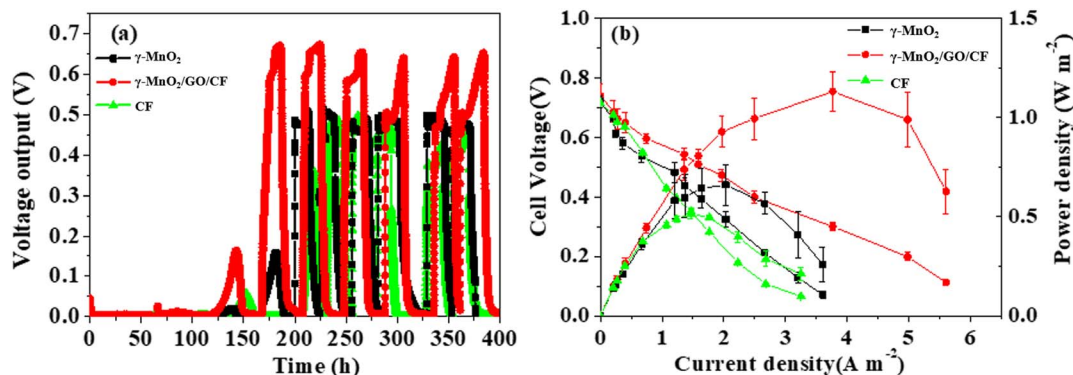
Fig. 5 Voltage output *versus* time during start-up of the MFCs with various anodes with 1000 Ω resistance loading (a); polarization curves and power densities of the MFCs with different anodes (b).

$Ni_{0.1}Mn_{0.9}O_{1.45}$/CF electrode in Table S1.† [5,8,11–14] It is attributed to a coating of the γ-MnO_2/GO composite on the CF anode, which combines the advantages of γ-MnO_2 and GO, can effectively enhance high conductivity, and offers a large surface area for bacterial adhesion, thereby greatly enhancing the anode performance.

2.3 Electrochemical activity

To confirm the anodic performance, Fig. 6a shows the bioelectrocatalytic current generation curves measured from the γ-

MnO_2/GO/CF and γ-MnO_2/CF anodes in half-batch experiments. The biofilm was cultivated in a half-cell setup under potentiostatic control. Under these conditions, the γ-MnO_2/GO/CF anode generated a higher current than the γ-MnO_2/CF and CF anodes. Furthermore, the potential responses shown in Fig. 6b were obtained under a constant current (0.1 μA), reflecting the polarization of the anodes. As previously reported, the more negative the plateau potential, the higher the anodic activity of the anode.[13,14] As depicted in Fig. 6b, the plateau potential of the γ-MnO_2/GO/CF anode (-0.53 V *vs.* SCE) is more
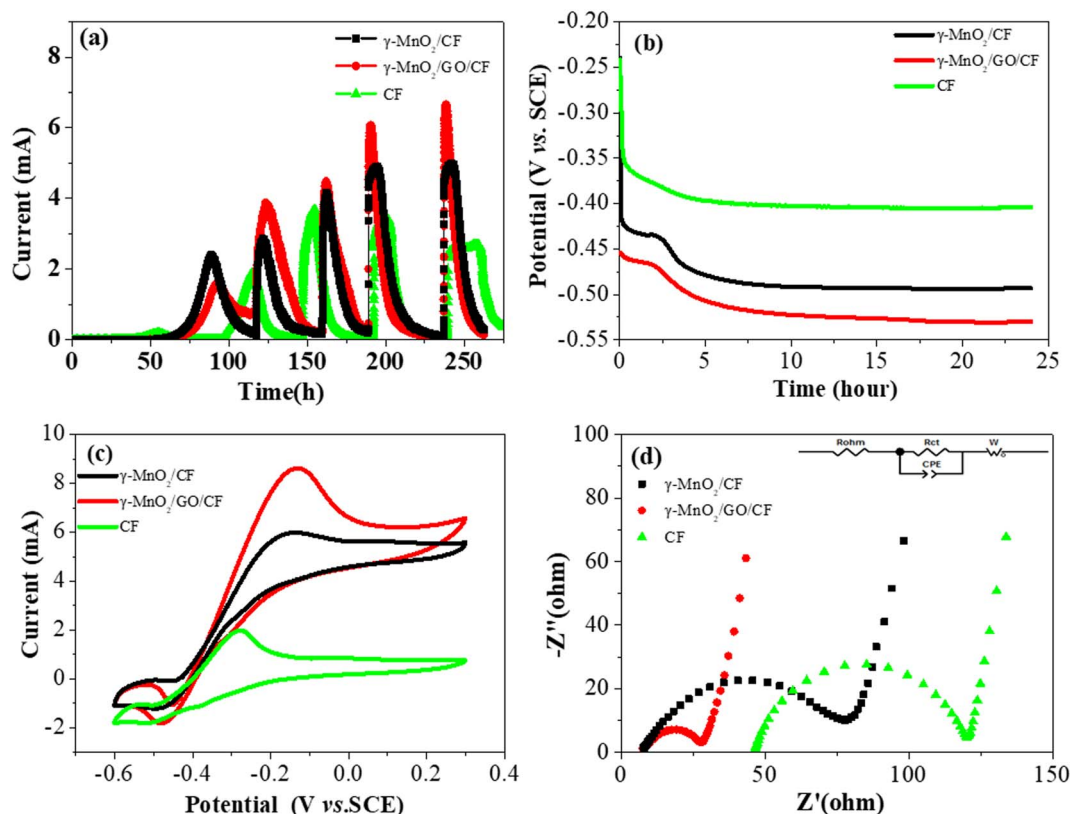

Fig. 6 Bioelectrocatalytic current generation at the γ-MnO_2/CF, γ-MnO_2/GO/CF and CF electrodes poised at 0.2 V (*vs.* SCE) (a); potential responses of various electrodes under a constant current of 0.1 μA (b); cyclic voltammograms for various electrodes after inoculation under turnover conditions (scan rate: 10 mV s^{-1}) (c); electrochemical impedance spectra of various electrodes after inoculation at the open circuit potential (Inset: equivalent circuit model) (d).

negative compared to those of the γ-MnO$_2$/CF (-0.49 V $vs.$ SCE) and CF (-0.4 V $vs.$ SCE) anodes, indicating that the γ-MnO$_2$/GO possesses better electrochemical activity. This may be because γ-MnO$_2$ exhibits superior biocompatibility and pseudocapacitive properties, which are conducive to bacterial adhesion, and enhanced electrode reaction and electron transfer.[18,19] Furthermore, the multilayer γ-MnO$_2$/GO nanoflake composite provides a large surface area for bacterial adhesion, consequently increasing the loading amount of bacteria and facilitating the EET between the anode and bacteria.

CV was utilized to further evaluate the electrochemical catalytic behaviour of γ-MnO$_2$/GO composite.[34] After 2 months of stable operation, CV curves were scanned under turnover conditions to study the bioelectrocatalytic activity of the electrodes. As depicted in Fig. 6c, after adding sodium acetate, S-shaped CV curves were observed from the anodes, indicating the catalytic oxidation of acetate by the electrodes. After being modified with the γ-MnO$_2$/GO composite, the peak current of

the modified electrodes was 1.5 and 4.3 times higher than those of the γ-MnO$_2$/CF and CF electrodes, respectively. The results demonstrate that γ-MnO$_2$/GO composite has excellent electrocatalytic activity, and the modification with the γ-MnO$_2$/GO composite improves the electron transfer efficiency from the bacteria to the anode. The CVs under non-turnover condition were used to determine the biocatalytic active sites of the biofilm.[35] As shown in Fig. S4,† the γ-MnO$_2$/GO/CF electrode displays a major redox couple with a potential of approximately -0.29 V and a shape similar to that of other electroactive biofilms, which can be attributed to two essential outer membrane c-type cytochromes, OmcB and OmcZ.[36] These cytochromes are essential for EET in MFCs.

To investigate the effect of γ-MnO$_2$/GO on the electron transfer kinetics between the anode and bacteria, EIS was conducted on the MFCs after inoculation. Fig. 6d presents the EIS spectra of the γ-MnO$_2$/GO/CF and γ-MnO$_2$/CF electrodes, with the inset showing the equivalent circuit model. The x-
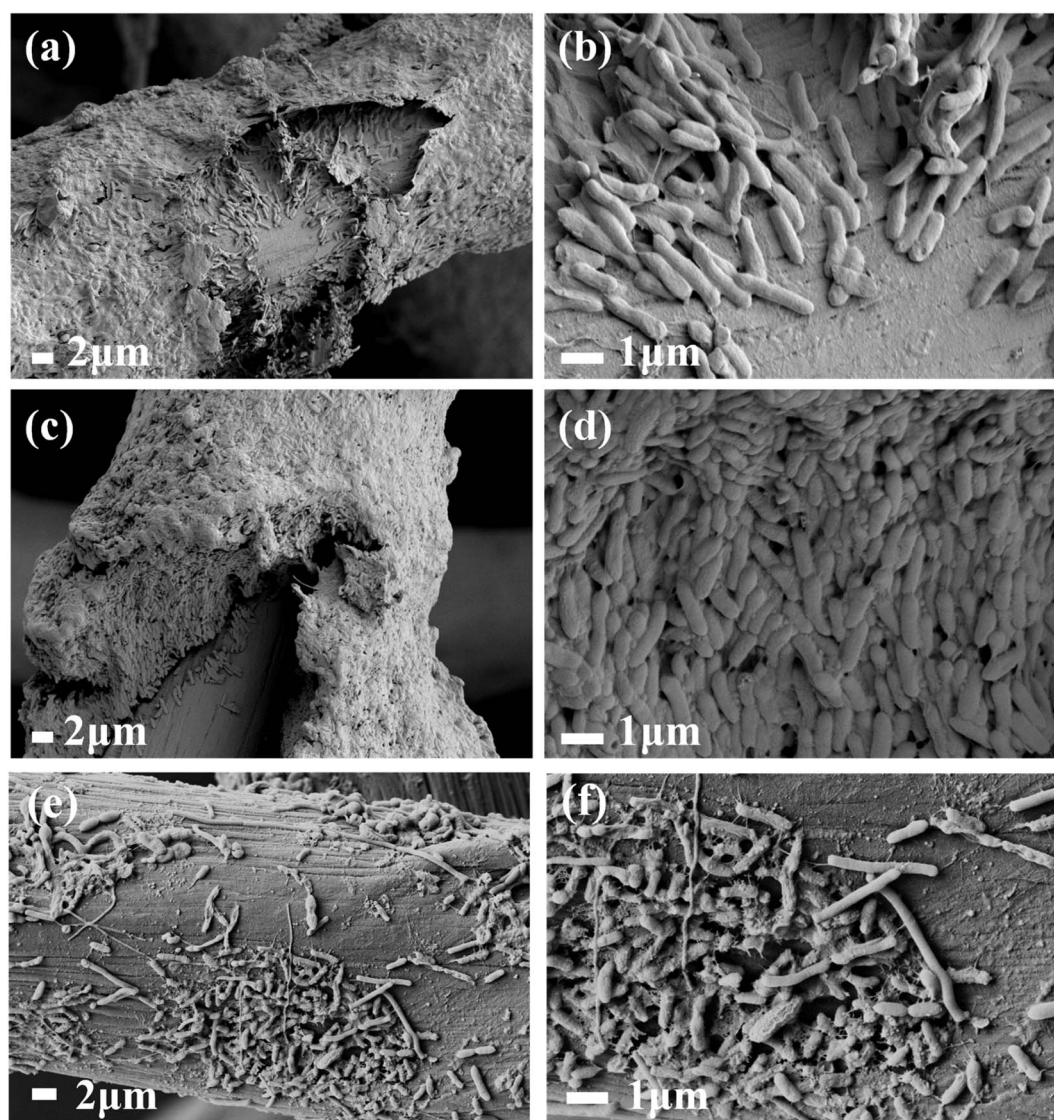
Fig. 7 SEM images of the electroactive biofilm grown on the γ-MnO$_2$/CF (a and b), γ-MnO$_2$/GO/CF (c and d), and CF (e and f) electrodes.

intercepts on the Nyquist curve reflects the ohmic resistance (R_{ohm}), and the charge-transfer resistance (R_{ct}) is determined by the diameter of the semicircular curve.[11,13] As shown in Fig. 6d, the R_{ohm} of γ-MnO$_2$/GO/CF and the γ-MnO$_2$/CF electrodes is similar, which is much smaller than that of the CF electrode (46.21 Ω). It is worth noting that the R_{ct} of the γ-MnO$_2$/GO/CF electrode (20.14 Ω) is less than those of the γ-MnO$_2$/CF electrode (69.80 Ω) and CF electrode (74.28 Ω). The results suggest that the γ-MnO$_2$/GO composite significantly enhances the electrochemical reaction rate, and reduces the electron transfer resistance between the bacteria and the anode.[19]

2.4 Biofilm of γ-MnO$_2$/GO/CF

The biocompatibility of the anode is an important factor affecting the performance of MFCs, as it directly affects the growth and attachment of bacteria to the anode surface, as well as the formation of biofilm.[3,15] The biofilm is responsible for the direct electron transfer between bacteria and the anode in MFCs.[37]

After 2 months of steady operation, the structure and morphology of the biofilm on the electrodes were characterized using SEM. As shown in Fig. 7, the biofilm on the γ-MnO$_2$/CF electrode (Fig. 7a and b) is much thinner than that on the γ-MnO$_2$/GO/CF electrode (Fig. 7c and d). The entire surface of the γ-MnO$_2$/GO/CF electrode is covered with a thick biofilm, with a thickness of up to 10 μm, and rod-shaped bacteria are closely packed together. Notably, only a few bacteria are found on the CF electrode (Fig. 7e and f) due to the smoothness of the CF electrode's surface. This is because γ-MnO$_2$ has good biocompatibility.[18,19] Furthermore, compared to the γ-MnO$_2$/CF and CF electrodes, the γ-MnO$_2$/GO/CF electrode has a rougher surface and a larger surface area, which makes it easier for bacterial growth and adhesion on the surface of the γ-MnO$_2$/GO/CF electrode. The results indicate that the γ-MnO$_2$/GO coating on the smooth surface of CF is conducive to enhancing the adhesion of bacteria and accelerating the EET from the bacteria to the electrode, which facilitates the formation of a biofilm on the electrode. Due to the stability of the biofilm, the MFC equipped with the γ-MnO$_2$/GO/CF anode achieves stable operation. The voltage outputs across a 1000 Ω resistor do not decay for 2 months. Moreover, after 2 months of operation, the γ-MnO$_2$/GO/CF electrode is not blocked by a thick biofilm.

The electron-transfer mechanism at the γ-MnO$_2$/GO/CF electrode is shown in Fig. S5.† The electrons generated by microbial metabolism are directly transferred to the γ-MnO$_2$/GO/CF electrode *via* direct contact or nanowires.[11] Due to the excellent biocompatibility and unique structure of the multilayer γ-MnO$_2$/GO nanoflakes composite, more bacterial cells are firmly adhered to the fiber surface through the electrostatic interaction between bacteria and the rough surfaces of the γ-MnO$_2$/GO composite (Fig. S5†), which facilitates the formation of an electroactive biofilm. In addition, the γ-MnO$_2$/GO composite possesses superior electrochemical activity, which can accelerate the transfer of electrons generated by metabolism to the electrode.

3 Conclusions

In summary, a novel multilayer nanoflake structure of the γ-MnO$_2$/GO composite has been fabricated *via* a simple template-free chemical precipitation method. The γ-MnO$_2$/GO composite-modified CF electrode has been used as an anode material for MFCs. The multilayer γ-MnO$_2$/GO nanoflake composite, with its unique multilayer nanoflake structure and superior biocompatibility, offers a large specific surface area for bacterial adhesion and exhibits excellent electrochemical performance. The MFC equipped with the γ-MnO$_2$/GO/CF anode achieves a maximum power density of 1.13 ± 0.09 W m^{-2}, which is 119% higher than that of the pure CF anode under the same conditions. This work introduces a facile method to fabricate multilayer γ-MnO$_2$/GO nanoflakes without the use of any template, and it is a promising anode material for high-performance MFCs applications.

Data availability

All data included in this study are available from the corresponding author upon request.

Conflicts of interest

There are no conflicts to declare.

Acknowledgements

References

1 M. H. Hu, X. Li, J. Xiong, L. Z. Zeng, Y. S. Huang, Y. P. Wu, G. Z. Cao and W. S. Li, *Biosens. Bioelectron.*, 2019, **142**, 111594.

2 A. Saravanan, P. S. Kumar, S. Srinivasan, S. Jeevanantham, R. Kamalesh and S. Karishma, *Chemosphere*, 2022, **290**, 133295.

3 A. Banerjee, R. K. Calay and M. Mustafa, *Energies*, 2022, **15**, 2283.

4 A. A. Yaqoob, M. N. M. Ibrahim and C. Guerrero-Barajas, *Environ. Technol. Innovation*, 2021, **23**, 101579.

5 L. H. Huang, X. F. Li, Y. P. Ren and X. H. Wang, *Int. J. Hydrogen Energy*, 2016, **41**, 11369–11379.

6 X. Xie, G. Yu, N. Liu, Z. Bao, C. Criddle and Y. Cui, *Energy Environ. Sci.*, 2012, **5**, 6862–6866.

7 X. Xie, M. Ye, L. B. Hu, N. Liu, J. R. McDonough, W. Chen, H. N. Alshareef, C. S. Criddle and Y. Cui, *Energy Environ. Sci.*, 2012, **5**, 5265–5270.

8 S. S. Chen, J. H. Tang, X. Y. Jing, Y. Liu, Y. Yuan and S. G. Zhou, *Electrochim. Acta*, 2016, **212**, 883–889.

9 S. Li, C. Cheng and A. Thomas, *Adv. Mater.*, 2017, **29**, 1602547.

10 J. M. Sonawane, A. Yadav, P. C. Ghosh and S. B. Adeloju, *Biosens. Bioelectron.*, 2017, **90**, 558–576.

11 L. Zeng, S. Zhao, L. Zhang and M. He, *RSC Adv.*, 2018, **8**, 40490–40497.

12 Y. Yuan, S. G. Zhou, Y. Liu and J. H. Tang, *Environ. Sci. Technol.*, 2013, **47**, 14525–14532.

13 L. Z. Zeng, S. F. Zhao and M. He, *J. Power Sources*, 2018, **376**, 33–40.

14 L. Z. Zeng, W. G. Zhang, P. Xia, W. Q. Tu, C. C. Ye and M. He, *Biosens. Bioelectron.*, 2018, **102**, 351–356.

15 Y. Q. Wang, B. Li, L. Z. Zeng, D. Cui, X. D. Xiang and W. S. Li, *Biosens. Bioelectron.*, 2013, **41**, 582–588.

16 Y. Xiao, J. Y. Hwang and Y. K. Sun, *J. Mater. Chem. A*, 2016, **4**, 10379–10393.

17 L. Z. Zeng, L. X. Zhang, W. S. Li, S. F. Zhao, J. F. Lei and Z. H. Zhou, *Biosens. Bioelectron.*, 2010, **25**, 2696–2700.

18 C. Y. Zhang, P. Liang, Y. Jiang and X. Huang, *J. Power Sources*, 2015, **273**, 580–583.

19 C. Y. Zhang, P. Liang, X. F. Yang, Y. Jiang, Y. H. Bian, C. M. Chen, X. Y. Zhang and X. Huang, *Biosens. Bioelectron.*, 2016, **81**, 32–38.

20 P. Xia, H. B. Lin, W. Q. Tu, X. Q. Chen, X. Cai, X. W. Zheng, M. Q. Xu and W. S. Li, *Electrochim. Acta*, 2016, **198**, 66–76.

21 Y. F. Zhao, W. Ran, J. He, Y. Z. Huang, Z. F. Liu, W. Liu, Y. F. Tong, L. Zhang, D. W. Gao and F. M. Gao, *Small*, 2015, **11**, 1310–1319.

22 Q. Zhang, X. F. Wu, Q. Q. Zhang, F. J. Yang, H. Z. Dong, J. Sui and L. F. Dong, *J. Electroanal. Chem.*, 2019, **837**, 108–115.

23 C. T. Hsieh, S. M. Hsu, J. Y. Lin and H. Teng, *J. Phys. Chem. C*, 2011, **115**, 12367–12374.

24 X. Y. Yang, X. Y. Zhang, Y. F. Ma, Y. Huang, Y. S. Wang and Y. S. Chen, *J. Mater. Chem.*, 2009, **19**, 2710–2714.

25 W. S. Hummers and R. E. Offeman, *J. Am. Chem. Soc.*, 1958, **80**, 1339.

26 C. Hontoria-Lucas, A. J. López-Peinado, J. López-González, D. De, M. L. Rojas-Cervantes and R. M. Martín-Aranda, *Carbon*, 1995, **33**, 1585–1592.

27 B. Logan, S. Chen, V. Watson and G. Estadt, *Environ. Sci. Technol.*, 2007, **41**, 3341–3346.

28 W. H. Ryu, J. Y. Eom, R. Z. Yin, D. W. Han, W. K. Kim and H. S. Kwon, *J. Mater. Chem.*, 2011, **21**, 15337–15342.

29 K. Palanisamy, Y. Kim, H. Kim, J. M. Kim and W. S. Yoon, *J. Power Sources*, 2015, **275**, 351–361.

30 S. Chen, J. W. Zhu, X. D. Wu, Q. F. Han and X. Wang, *ACS Nano*, 2010, **4**, 2822–2830.

31 J. X. Hou, Z. L. Liu, S. Q. Yang and Yu. Zhou, *J. Power Sources*, 2014, **258**, 204–209.

32 Q. Yang, Q. Li, Z. Yan, X. N. Hu, L. P. Kang, Z. B. Lei and Z. H. Liu, *Electrochim. Acta*, 2014, **129**, 237–244.

33 R. I. Jafri, N. Rajalakshmi and S. Ramaprabhu, *J. Mater. Chem.*, 2010, **20**, 7114–7117.

34 S. G. Zhou, J. H. Tang and Y. Yuan, *Bioelectrochem*, 2015, **102**, 29–34.

35 K. Guo, S. Freguia, P. G. Dennis, X. Chen, B. C. Donose, J. Keller, J. J. Gooding and K. Rabaey, *Environ. Sci. Technol.*, 2013, **47**, 7563–7570.

36 Y. Liu, F. Harnisch, K. Fricke, R. Sietmann and U. Schröder, *Biosens. Bioelectron.*, 2008, **24**, 1006–1011.

37 B. A. Hemdan, D. A. Jadhav, A. Dutta and P. Goswami, *J. Water Process Eng.*, 2023, **54**, 104065.